Atmospheric Pressure Plasma CVD of Amorphous Hydrogenated Silicon Carbonitride (a-SiCN:H) Films Using Triethylsilane and Nitrogen

Srinivasan Guruvenket,* Steven Andrie, Mark Simon, Kyle W. Johnson, Robert A. Sailer

Amorphous hydrogenated silicon carbonitride (a-SiCN:H) thin films are synthesized by atmospheric pressure plasma enhanced chemical vapor (AP-PECVD) deposition using the Surfx Atomflow™ 250D APPJ source with triethylsilane ($HSiEt_3$, TES) and nitrogen as the precursor and the reactive gases, respectively. The effect of the substrate temperature (T_s) on the growth characteristics and the properties of a-SiCN:H films was evaluated. The properties of the films were investigated *via* scanning electron microscopy (SEM), atomic force microscopy (AFM) for surface morphological analyses, Fourier transform infrared spectroscopy (FTIR), and X-ray photoelectron spectroscopy (XPS) for chemical and compositional analyses; spectroscopic ellipsometry for optical properties and thickness determination and nanoindentation to determine the mechanical properties of the a-SiCN:H films. Films deposited at low T_s depict organic like features, while the films deposited at high T_s depict ceramic like features. FTIR and XPS studies reveal that an increases in T_s helps in the elimination of organic moieties and incorporation of nitrogen in the film. Films deposited at T_s of 425 °C have an index of refraction (n) of 1.84 and hardness (H) of 14. 8 GPa. A decrease in the deposition rate between T_s of 25 and 250 °C and increase in deposition rate between T_s of 250 and 425 °C indicate that the growth of a-SiCN:H films at lower T_s are surface reaction controlled, while at high temperatures film growth is mass-transport controlled. Based on the experimental results, a potential route for film growth is proposed.

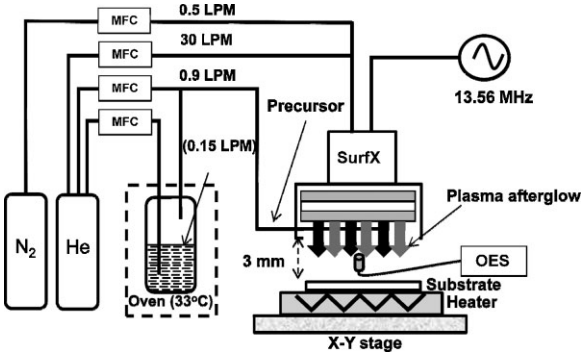

S. Guruvenket, R. A. Sailer
Center for Nanoscale Science and Engineering, North Dakota State University, Research Park Drive, Fargo, North Dakota 58102, USA
Fax: +1 701 231 5306; E-mail: guruvenket.srinivasan@ndsu.edu
S. Andrie, M. Simon, K. W. Johnson
Department of Mechanical Engineering, North Dakota State University, 111 Dolve Hall, Fargo, North Dakota 58102, USA

1. Introduction

Amorphous thin films of silicon such as silicon nitride (a-SiN:H), silicon carbide (a-SiC:H), silicon carbonitride (a-SiCN:H), etc. find applications as protective coatings, dielectric gate layers in microelectronics applications, and optical coatings such as anti-reflection coatings in solar cells, etc.[1–4] Plasma enhanced chemical vapor deposition

DOI: 10.1002/ppap.201100035

(PECVD) is a widely used technique to synthesize these coatings, which utilizes hazardous chemicals like silane, ammonia, and/or methane at low pressures.[4] Typical low-pressure direct PECVD (D-PECVD) processes utilize electron-initiated mechanisms to cause fragmentation of the precursor molecules. This is followed by gas phase reactions among the fragmented molecules to form active radicals that lead to film formation on the substrate. In D-PECVD, the substrate is immersed in the plasma and undergoes ion bombardment leading to undesired residual stress in the deposited thin films.[5] This residual stress can be minimized by using a remote PECVD (R-PECVD) process, where the precursor reacts with the reactive radicals in the region that is isolated from the energetic ions and electrons. Wrobel and coworkers[6–10] used a R-PECVD process with various metal-organic precursor sources with different gas compositions to form the afore-mentioned Si based thin films at low-pressures.

Facilitation of PECVD processes at atmospheric pressure which make use of non-hazardous chemicals (precursors) will find effectiveness in a continuous manufacturing environment, where rewards are foreseen in terms of higher throughput and lower costs (i.e., capital and operational). In the recent past, there has been an increasing interest in utilizing atmospheric pressure plasma (APP) based surface processing methods for surface activation (cleaning), plasma polymerization and atmospheric pressure PECVD (AP-PECVD).[11–13] Bárdos and Baránková[14] in their recent article summarized some examples of thin film metal oxides, plasma polymers and diamond-like carbon (DLC) materials deposited using AP-PECVD. Interesting observations were made by several researchers that good quality thin films at atmospheric pressure could be synthesized by optimizing the processing conditions (i.e., precursor and reactive gas chemistries, plasma power, substrate temperature, etc). Raballand et al.,[15] demonstrated the deposition of SiO_2 and SiOC thin films using organosilanes such as trimethylsilane and hexamethylydisiloxane (HMDSO) by tuning the reactive gas concentration and the plasma power density. The same authors observed SiO_2 films free of carbon when the HMDSO flow was balanced with reactive O_2 gas.[16] Hopfe and Sheel[17,18] and Hopfe et al.,[19] deposited good-quality SiN_x films using a linear extended DC arc reactor with mixtures of SiH_4, $HSi(CH_3)_3$, N_2, and NH_3 gases. Nowling et al.,[20,21] and Ladwig et al.,[22] demonstrated the deposition of SiN_x using He–SiH_4–N_2 mixtures and DLC using He–CH_4 mixtures, respectively, using Surfx Atomflow^{TM} 250D-APPJ. Earlier, we reported the use of AP-PECVD processing to form SnO_x, In:SnO_x, ZnO, and Al:ZnO coatings, where we established that the deposited film's properties strongly depend on the chemistry of the precursors, the reactive gas chemistries and the other processing conditions.[23–25]

Despite several reports on AP-PECVD, the interrelationships between the plasma properties, precursor chemistries, growth conditions, and their effect on film properties are not well understood. In this article we report the use of triethylsilane ($HSiEt_3$) and nitrogen to form a-SiCN:H thin films at atmospheric pressure using Surfx Atomflow^{TM} 250D APPJ source. The fundamental processes underlying film growth were elucidated from the thin film's properties; plasma characterization will also be discussed.

2. Experimental Section

2.1. Deposition of a-SiCN:H Coatings

Thin films of a-SiCN:H were deposited using a Surfx Atomflow^{TM}250D APPJ system described elsewhere.[25–27] A schematic representation of the AP-PECVD system and the precursor delivery is shown in Figure 1. $HSiEt_3$, was used as the precursor which is a liquid at standard temperature and pressure (b.p. 117–118 °C). TES has a significant vapor pressure ($P_v = 23$ Torr at 20 °C, used as received from Gelest, USA). $HSiEt_3$ was delivered to the plasma source from a heated bubbler maintained at 33 °C (to increase vapor pressure). In order to preclude the precursor condensation, the delivery lines were maintained at 100 °C and the plasma head was held at 125°C. Helium and N_2 were used as the plasma and reactive gases, respectively, and their flows were maintained at 30 and 0.5 lpm, respectively, while the precursor carrier gas (He) flow was kept at 0.15 lpm through the precursor bubbler. The flow path of the precursor, plasma gas and the reactive gas are illustrated in Figure 1. In this investigation plasma power was held a constant at 120 ± 10 W, while the substrate temperature (T_s) was varied between the room temperature (RT, 25) and 425 °C. The substrate to plasma distance was fixed at 3 mm. Crystalline double-side polished intrinsic Si wafers (2.5×2.5 cm^2) cleaned with isopropyl alcohol were used as the substrates. Depositions were carried out by moving the heated substrate holder (platen) under the plasma source in a serpentine motion. The serpentine motion parameters (length, width, step size, and velocity) were chosen to produce uniform film deposition across the entire substrate surface. In order

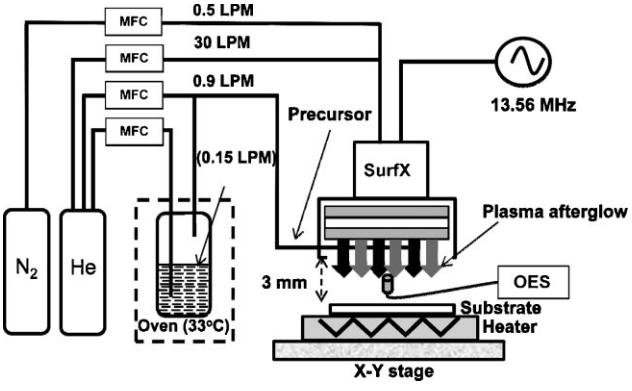

Figure 1. Schematic representation of AP-PECVD system with Surfx^{TM} 200 (Atomflo).

DOI: 10.1002/ppap.201100035

to preclude oxygen contamination, the plasma source was located inside an inert atmosphere (glove box filled with nitrogen).

2.2. Plasma and Thin Film Characterization

Optical emission spectroscopic (OES) analyses were performed using an Ocean Optics SD 2000 spectrophotometer coupled with an optical fiber to characterize the afterglow region of the Surfx^{TM} 250 D plasma source as illustrated in Figure 1. The optical fiber was placed along the axis of the plasma source at ~3 mm to collect the light intensity normal to the electrode. OES spectra were measured between 180 and 890 nm with a resolution of 0.4 nm.

Surface morphology of the films was investigated using JEOL JSM 7600F high resolution scanning electron microscope (SEM) equipped with a field emission gun. To avoid surface charging, samples were coated with ~10 nm of conducting layer, while secondary electrons were used to map the surface morphology of the coatings. In order to compliment the SEM analysis and to obtain quantitative details on the surface roughness Atomic force microscopy (AFM) studies were performed using Veeco DI-3100 instrument in tapping mode.

To investigate the chemical (bonding) structure of the films, Fourier transform infrared spectroscopy (FTIR) was performed using a Thermo Scientific Nicolet 8700 instrument, and X-ray photoelectron spectroscopy (XPS) measurements were performed on a Surface Science Instruments (SSX-100) equipped with a monochromatic Al Kα source, a hemispherical sector analyzer (HAS), and a resistive anode detector. The base pressure and pressure during data collection were 10^{-9} and 10^{-8} Torr, respectively. Survey and high resolution scans were performed to determine the elemental composition and their chemical structure, respectively.

Optical constants of the films were determined using a J. A. Woollam VASE spectroscopic ellipsometer with modeling and data analyses realized using WVASE software package. Ellipsometric Ψ and Δ data were acquired at three angles of incidence (60°, 67°, and 74°) over the spectral range 300–780 nm in steps of 10 nm. Optical constants and the thickness of the films were determined by modeling a thin film on a Si substrate.

Hardness (H) and reduced Young's modulus (E_r) of the coatings were determined by depth sensitive indentation using a Triboindenter (Hysitron Inc.) system equipped with a Berkovich pyramidal tip. The applied loads ranged between 1 and 5 mN. For each sample, H and E_r were obtained from the average of 20 indentations using the method proposed by Oliver and Pharr.[28] Care has been taken in selecting the maximum load to ensure the measurements were performed at within 10% of the film thickness to avoid the substrate effect.

3. Results and Discussion

In this study, the effect of T_s on the properties of a-SiCN:H films were investigated. Films were deposited by varying T_s between 25 and 425 °C, and their microstructural, chemical, optical, and mechanical properties were examined. Experiments depicted no film formation without N_2 addition to the plasma gas (He) showing AP-PECVD is a radical initiated process and hence 500 sccm of N_2 flow was maintained.

Surface topography and the roughness of the a-SiCN:H films were analyzed via SEM and AFM, respectively. Figure 2a and b shows the SEM surface features of the a-SiCH surface deposited at 25 and 425 °C, respectively. It can be observed that the films deposited at 25 °C show

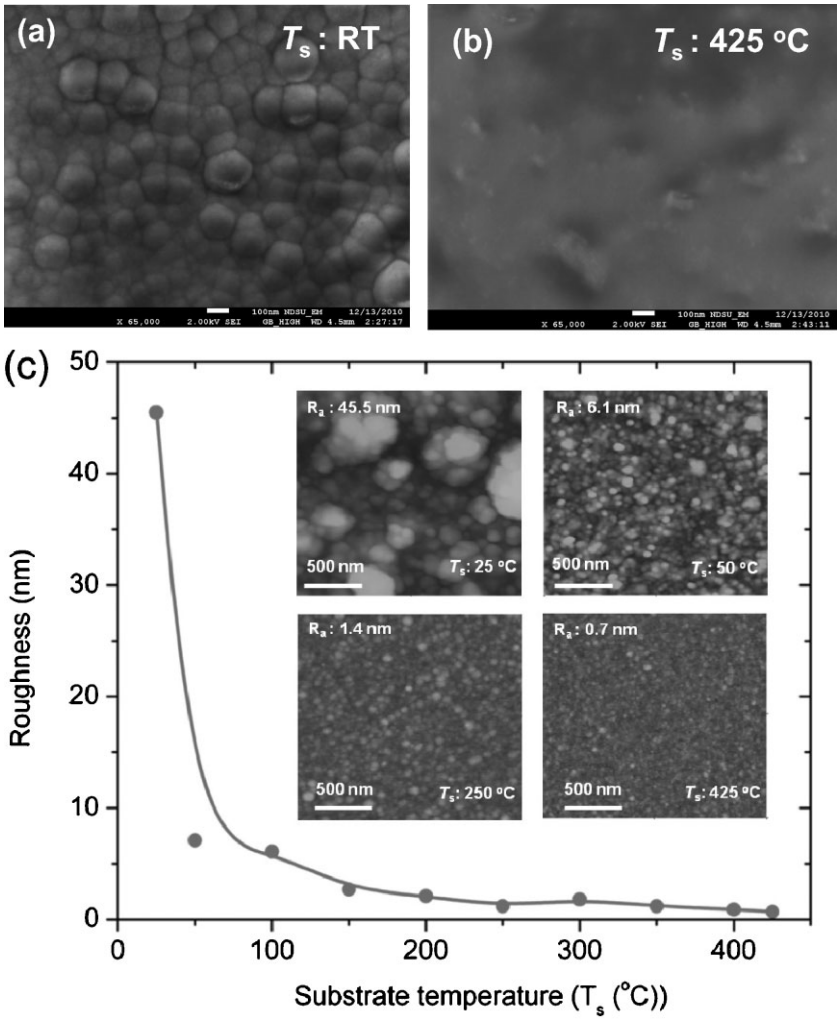

Figure 2. (a) and (b) SEM surface morphology of the a-SiCN:H films deposited at RT and 425 °C, respectively and (c) change in R_a *versus* T_s (inset: AFM surface topography).

collections of "globule-like" rough features, while the film deposited at 425 °C shows no such features. In order to obtain more quantitative roughness values and surface features, AFM measurements were performed and the average surface roughness (R_a) and surface features as a function of T_s are presented in Figure 2c and its inset, respectively. As observed in Figure 2c and its inset, films deposited at 25 °C show rough, agglomerated, globule-like features with R_a of 45.5 nm. With an increase in the T_s, globule-like features could not be observed and a decrease in the R_a from 45.5 to 0.5 nm (at T_s: 425 °C) was noted. The R_a values observed for films deposited at $T_s > 300$ °C are comparable to the R_a observed for SiN_x films obtained using PVD, PECVD and CVD techniques.[29–31] High R_a at low T_s and low R_a at high T_s suggest substrate temperatures induce chemical reactions at the growing surface leading to lower roughness. Thin film growth at the low temperatures can be viewed as Volmer–Weber mode (island growth) where the incoming species get absorbed (without any random diffusive jumps) on the substrate leading to porous features as depicted by SEM and AFM morphological studies. While on the other hand, an increase in T_s offers more energy to the incoming adatoms/admolecules as well as decreasing the surface energy (with 1 °C increase in T_s, ~0.05 mJ decrease in surface energy is typical) leading to a possible Frank–Vander Merwe (layer by layer) growth mode.[32]

Chemical structures of the films were investigated using FTIR spectroscopic analyses which provided important and interesting results. Figure 3 depicts FTIR spectra of the films deposited at T_s from 25 to 425 °C. a-SiCN:H films synthesized at 25–150 °C depict similar features with absorptions bands at ~1 030–1 050 cm^{-1} and 2 880–2 960 cm^{-1} corresponding to Si–$(CH_2)_n$–Si or Si–O, and CH_n ($n = 1$–3), respectively. Weak absorption peaks at 1 240, 1 170, 2 050–2 010 and 3 890 cm^{-1} corresponding to Si–Et_n, Si–NH–Si(C), Si–H_n ($n = 1, 2$), and N–H_n groups were also observed.[33–36] Films deposited at 200 °C exhibit similar characteristic absorption peaks except absorption intensity corresponding to CH_n bonds (2 880–2 960 cm^{-1}) which decreased with a concurrent increase in the Si–NH–Si(C) related group at 1 170 cm^{-1}. Films deposited at T_s of 250 °C exhibited significant changes in the IR spectra with absorptions corresponding to Si–H_n vibrations at ~915 and ~2 150 cm^{-1} along with Si–C (carbidic) and Si–N bonds at ~780 and ~860 cm^{-1}, respectively. The vibration at 915 cm^{-1} can also be attributed to the Si–CH_n bonds.[37,38] A significant decrease in the intensity of Si–$(CH_2)_n$–Si at 1 030 cm^{-1} and Si–Et_3 (~1 250 cm^{-1}) groups was also detected. The broad peak between 2 050 and 2 300 cm^{-1} could be due to the combined effect of Si–H_n (2 050–2 150 cm^{-1}) and C–N (2 200 cm^{-1}) bonds, which is supported by the XPS results (presented in a later section).[1,29] Film deposited at 300 °C exhibited similar characteristic features. At T_s above 350 °C the films showed a decrease in the absorption corresponding to Si–H_n vibrations at (~2 150 and at 915 cm^{-1}), with significant peak broadening between 700 and 1 100 cm^{-1}. This broad peak at ~920 cm^{-1} could be attributed to the overlap of many components including Si–H_n and/or Si–CH_n at 915–940 cm^{-1} and Si–N at 860 cm^{-1}. With an increase in T_s to 400 and 425 °C, no significant change in the chemical features was noticed except that Si–H_n (2 150 cm^{-1}) became insignificant, while the broad peak centered ~920 cm^{-1} grew in significance. Based on the decrease in Si–H_n vibration at 2 150 cm^{-1}, it can be concluded that the Si–H_n peak had little contribution to the broad peak (~920 cm^{-1}), which indicated higher fraction of Si–C and Si–N bonds with an increase in T_s.

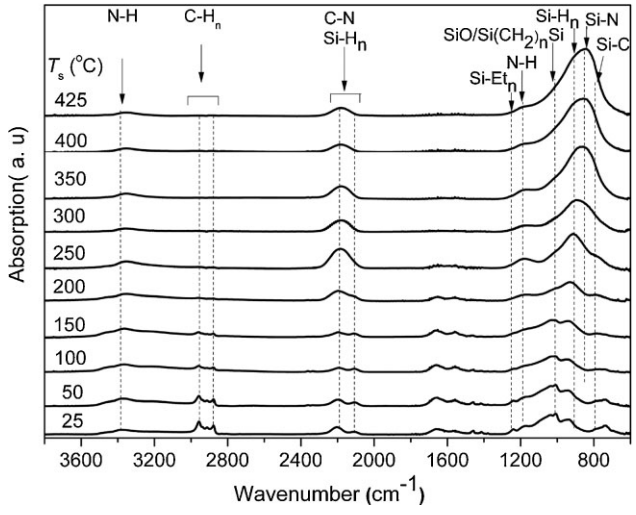

Figure 3. FTIR spectra of a-SiCN:H thin films deposited at T_s from 25 to 425 °C.

These observations imply thermally induced reactions between plasma activated $HSiEt_3$ and the nitrogen species on the substrate surface leading to a-SiCN:H film with different chemical features depending on the T_s. A detailed chemical route for the film formation is explained in a later section.

In order to determine the elemental composition and the chemical states of the elements present in the films, XPS studies were performed. Atomic percentage of the elements present in the thin films deposited at 25, 150, 250, 350, and 425 °C were determined using survey scans and are shown in Table 1. Films deposited at 25 °C exhibit the highest concentration of oxygen (27.8 at.%), which decreases gradually with an increase in T_s as depicted in Table 1. a-SiCN:H films deposited below 150 °C show 21–31 at.% of carbon and nitrogen ≥14.9 at.%. With an increase in T_s to 250 °C and above, the carbon content in the film gradually decreases, while the nitrogen concentration is increased as depicted in Table 1. a-SiCN:H films deposited at 425 °C showed 51.9 at.% of Si, 34.6 at.% of N, 4.8 at.% of C, and 8.7 at.% of O. With an increase in T_s the amount of nitrogen

DOI: 10.1002/ppap.201100035

Table 1. Elemental composition of a-SiCN:H films.

T_s(°C)	Elemental composition (at.%)			
	Si	C	N	O
25	34.9	30.6	6.7	27.8
150	42.6	21.2	14.9	21.3
250	43.9	5.9	33.4	16.8
350	49.7	6.9	31.8	11.6
425	51.9	4.8	34.6	8.7

incorporated in the film increased with a concurrent decrease in the carbon concentration. The higher concentration of oxygen present in the films deposited at low T_s can be attributed to the post-deposition reactions between the film and ambient oxygen due to the organic nature of the film. On the other hand the films deposited at higher T_s contained lower oxygen content implying possible oxygen reaction during the film synthesis (oxygen contamination could be from the precursor, gases used, and/or the residual oxygen present in the glove box).

Chemical states of the elements present in the a-SiCN:H films were determined using the Si 2p, C 1s, N 1s, and O 1s core level spectra (depicted in Figure 4). From the Si 2p spectra (Figure 5a) it can be noted that as T_s increases, the bonding state of Si down shifts from 103 to 101.7 and 100.4 eV corresponding to Si–O, Si–N, and Si–C bonding states, respectively.[39,40] At T_s, 350 °C and above, peak broadening and shift in the peak position towards lower B. E could be observed. Such peak shifts are attributed to the presence of N and C complexes attached to the Si bonding site in a-SiCN.[41,42] An increase in Si–Si bonds (at 99.9 eV) was also observed for the films deposited at $T_s > 350$ °C, which is indicative of a possible detachment of the ethylene group from the parent TES molecule leading to increased Si–Si cross-linking.

The C 1s core level spectra of a-SiCN:H films as the function of T_s is depicted in Figure 4b. The C 1s spectra exhibited a predominant presence of C=C bonds at 285 eV; however with an increase in T_s from 25 to 350 °C, an increase in C–Si contribution (283.3 eV) was noticed. Further increase in T_s to 425 °C showed contributions from C–N and C=N at 286 and 287 eV, respectively, in addition to C–Si bonds with a simultaneous peak broadening.[39]

The N 1s spectra illustrates interesting properties; at low T_s (<250 °C) the spectra exhibits the presence of N=C (399.2 eV) and N–O (at 400.3 eV) bonds that signify nitrogen reaction with carbon in the ethyl group of TES radical and the stray oxygen present in the reactor. With an increase in $T_s > 250$ °C a gradual down shift in B. E from 399.2 to 397.3 eV (N–Si) and peak broadening was observed indicating N–Si and N–C bond formation with marked decrease in N–O contribution.[39,41,42] This indicated the

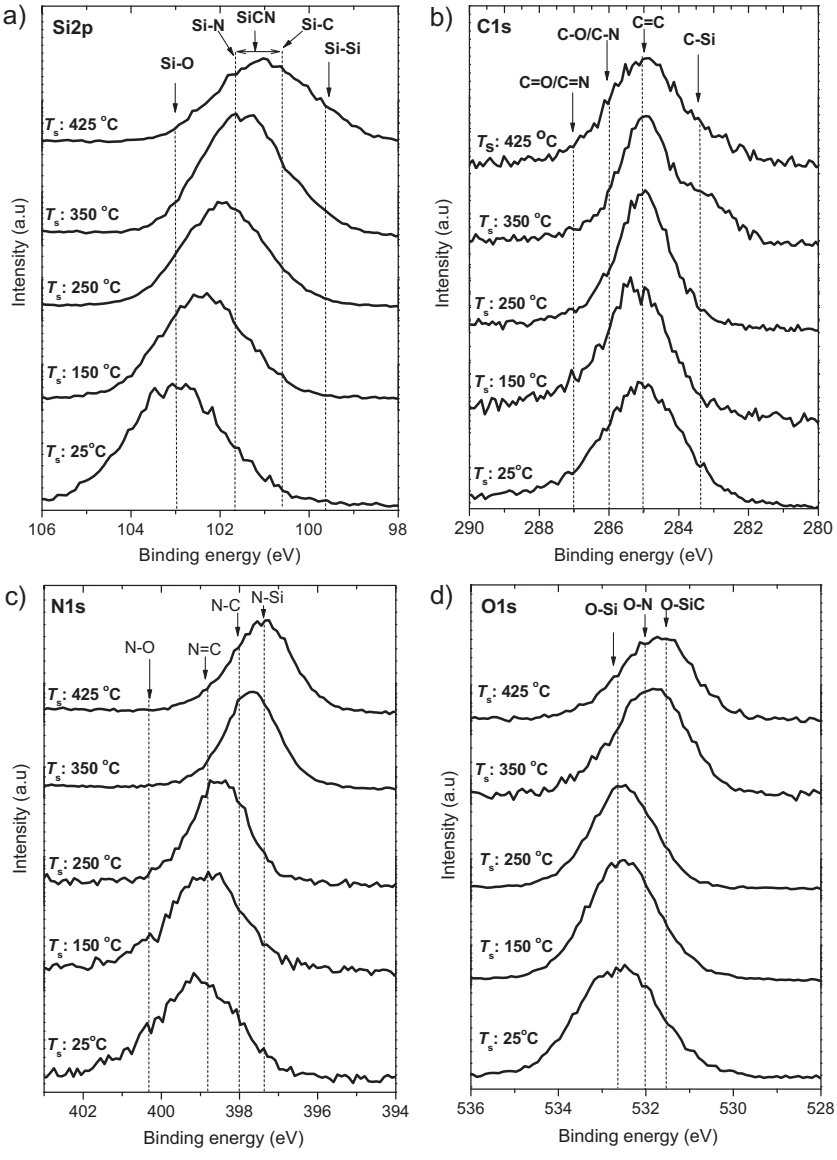

Figure 4. High resolution core level XPS spectra of a-SiCN:H films deposited a function of T_s; (a) Si 2p, (b) C 1s, (c) N 1s and (d) O 1s.

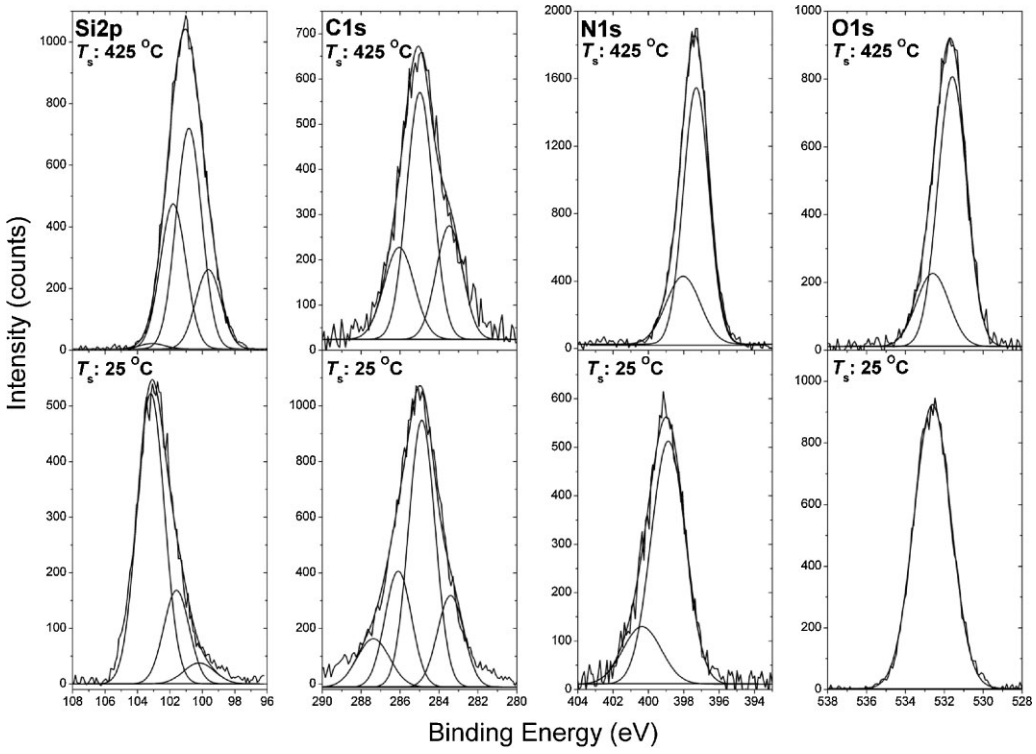

Figure 5. Deconvolution of Si 2p, C 1s, N 1s and O 1s spectra of a-SiCN:H films synthesized at T_s of 25 and 425 °C.

possibility of nitrogen reacting at the Si sites that could be formed due to the thermally induced ethyl group detachment from $SiEt_3$ radical. The above statement is validated by the appearance of Si–Si and Si–N from Si 2p core level spectra. From the O 1s spectra (Figure 4d) it can be seen that at $T_s \leq 250$ °C, oxygen was predominately bonded to Si and at $T_s > 250$ °C additional contributions from O–N and O–SiC could be noticed. Peak broadening observed in Si 2p, C 1s, N 1s and O 1s core levels for the films deposited at $T_s \geq 350$ °C could be attributed to the presence of several complex bonds in a-SiCN films as reported previously by several authors.[39–42]

Quantitative information was obtained by deconvoluting the Si 2p, C 1s, N 1s, and O 1s core level spectral bands. Representative deconvoluted spectral features for the core levels for the films deposited at 25 and 425 °C are depicted in Figure 6. The area under the curve for the individual component contributing to the collective core level elemental spectra is summarized in Table 2. For the films deposited at 25 °C, Si 2p depicts strong contribution from Si–O (~80.2%) Si–N (8.0%) and Si–C (11.8%) bonds, with the presence of small amounts of N–C and N–O as observed from the C 1s and N 1s spectra, respectively. With a gradual increase in T_s, a decrease in Si–O contribution and an increase in Si–C and Si–N bonds were observed. At $T_s = 425$ °C, 47.3% of Si–C, 40.4% of Si–N, and 10.5% of Si–Si bond contributions were calculated from area under the curve. Simultaneously from N 1s spectral analyses, an increase in the N–Si bonds, with a gradual decrease in N–C bonds was noticed, indicative of N–Si bond formation, which could be attributed to two simultaneous reactions; (i) evolution of ethyl groups (that were bonded to Si) and (ii) nitrogen atoms (from the plasma) reacting with Si resulting in Si–N bonds. The above statements are also supported by the concurrent increase in the Si–Si bonds representing enhanced surface cross-linking reactions via elimination of organic moieties as T_s increases. At T_s of

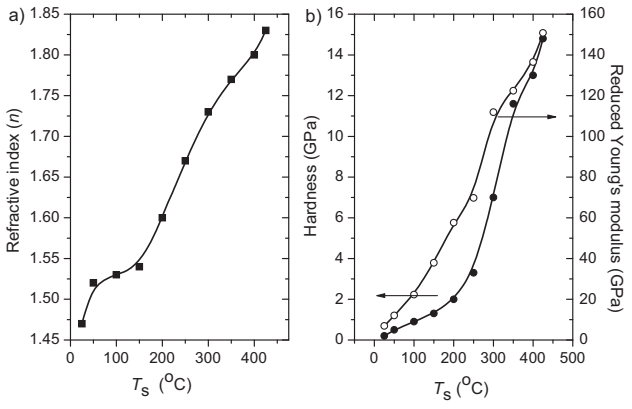

Figure 6. (a) Change in refractive index (n) as function of substrate temperature (b) H and E_r as the function of T_s.

DOI: 10.1002/ppap.201100035

Table 2. Peak position and deconvoluted area of C 1s, Si 2p and N 1s peaks from a-SiCN:H films.

T_s (°C)	Si 2p peak (eV)				C 1s peak (eV)				N 1s peak (eV)		
	Si–O	Si–C	Si–N	Si–Si	C–Si	C–C	C–N/C–O	C=N/C=O	N–Si	N–C/N=C	N–O
	103.0	100.4	101.7	99.9	283.3	285.0	286.0	287.0	397.3	398-399.2	400.3
25	80.2	11.8	8.0	—	19.5	50.9	16.6	13.0	—	79.1	20.9
150	40.4	50.2	9.4	—	8.6	55.0	36.4	—	—	86.5	13.5
250	10.5	46.4	38.4	4.7	10.4	68.9	20.7	—	8.3	84.8	6.9
350	6.5	21.9	65.5	6.1	27.4	53.7	18.9	—	51.6	41.1	7.3
425	1.8	47.3	40.4	10.5	24.4	53.2	22.4	—	73.9	26.1	—

425 °C, 73.9% of N–Si and 26.1% of N–C bond formation were observed from N 1s spectra deconvolution. A significant increase in the intensity of the Si 2p and N 1s peaks, with a simultaneous decrease in the C 1s and O 1s peak intensities as a function of increased T_s supported the formation of a Si–N rich a-SiCN:H network consisting of Si–C bonds. These results are also in agreement with the observations made by FTIR analysis.

Index of refraction (n) and the thickness of the films were determined using spectroscopic ellipsometry. Figure 5a depicts n as a function of T_s. Films deposited at $T_s < 150$ °C showed n lower than 1.54, while with an increase in T_s above 150 °C a gradual increase in n could be observed. At $T_s = 425$ °C, n of 1.84 was observed. Figure 6b shows H and E_r determined using nanoindentation as a function of T_s. Films deposited at RT depict low H and E_r of 0.2 and 6.9 GPa, respectively, while with an increase in T_s a gradual increase in H and E_r could be noticed and at $T_s = 425$ °C, H of 14.8 GPa and E_r of 150.8 GPa were observed.

The n, H, and E_r values observed for the a-SiCN:H films that were deposited at T_s above 300 °C are comparable to the films deposited with vacuum based processes.[1,36,39] In accordance with the FTIR and XPS results presented earlier the increase in n can be attributed to the formation of ceramic like a-SiCN phase which possess higher nitrogen content than the films that were deposited at lower temperatures. Another reason for the increase in n could be due to the increase in the film density as the function of substrate temperature. A similar increase in n for the a-SiN_x, a-SiC:H, and a-SiCN:H films were reported as the function of ion-bombardment or T_s for the films deposited using vacuum based plasma process such as sputtering and PECVD.[29,39,43] The increase in H and E_r can also be attributed to the increase in the density of the films, with a concurrent change occurring in the elemental concentration and the film microstructure as observed from the FTIR and XPS analysis (which depicts the change in film structure from organic to ceramic structure as the function of T_s).

Figure 7 depicts thickness based growth rate of a-SiCN:H films as the function of 1 000/T_s (K^{-1}). The change in the film thickness as the function of T_s is presented in the inset of Figure 7. With an increases in T_s from 25 °C, a gradual decrease in film thickness from 823 to 120 nm (at 250 °C) was observed, while an increase in T_s above 250 °C showed an increase in the film thickness to 200 nm at 425 °C. Growth rates plotted as 1 000/T_s depict positive and negative slopes between 25–250 °C and 250–425 °C, respectively. Decreasing slope (decrease in the film thickness) can be attributed to the thermally activated desorption of organic moieties (CH_n) from the adsorbed species on the substrate and enhanced surface diffusion of the adsorbed molecules leading to smooth denser films, which is supported by the increasing trend in n, H, and E_r values measured for the films deposited in this regime as explained earlier.[43] With an increase in T_s above 250 °C the combination of thermally induced desorption of organic moieties at the substrate surface, improved chemical

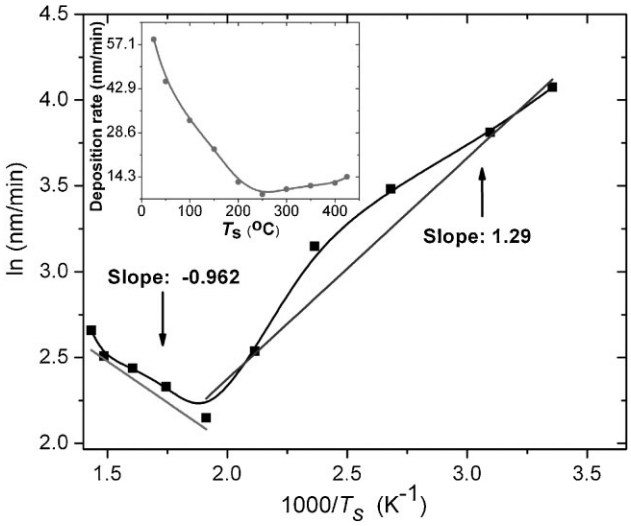

Figure 7. Deposition rate (logarithmic) as the function of 1 000/T_s (K^{-1}) and change in film thickness as a function of T_s (inset).

reactions between the adsorbed species with the growing film, along with higher adatom surface mobility are expected to enhance the formation of more dense, ceramic like films at higher growth rates, which was supported by the experimental observations (such as increase in nitrogen content with decrease in the carbon, and with an increase in n, H, E_r, and a decrease in R_a). Saturation in the growth rates beyond critical T_s is typical for thermally induced CVD process, in our case no such saturation was observed up to 425 °C.[32]

In a typical CVD process the growth rate ($\dot{G}$) can be expressed by the equation $\dot{G} = (K_g h_g C_g)/(K_g + h_g)N_o$, where k_s is the reaction rate, C_g is the concentration of reactant flux in the bulk gas, h_g is the mass transfer coefficient, and N_o is the atomic density of the thin film.[32] At low T_s, reaction rate (k_s) controls the film growth (surface reaction controlled), on the other hand at high T_s mass-transfer (h_g) controls the film growth. Gas phase diffusion of radicals depends on the pressure and temperature according to the relation $\sim T^{3/2}/P$.[32] In this study, since pressure was maintained a constant during the deposition, an increase in T_s will favor more gas-phase diffusion of precursor molecule/radicals towards the substrate. Also, as a function of T_s the surface reaction rate increased in accordance with Arrhenius behavior that is explained by the relation $k_s = [\exp(-E/RT_s)]$, where E is the activation energy and R is gas constant.[44] This is indicative of an enhanced reaction between the adsorbed species at higher temperatures, supported by the increase in nitrogen and decrease in carbon content of a-SiCN:H films deposited at high T_s (result of plasma activated nitrogen species reaction with $SiEt_3$ radicals on the substrate). These two processes (enhanced reactivity and higher radical diffusion) are accounted for the increase in film thickness for T_s ranging from 250 to 425 °C. Jumping frequency (Γ) of the adsorbed molecular species is directly proportional to α $[\exp(-E_{diff}/RT_s)]$. With an increase in T_s the jumping frequency increases, allowing higher root mean square displacement of the adsorbed species on the surface, hence leading to an energetically favorable position to form a stable film.[32] Also a slight decrease in the surface energy with increase in T_s assists the surface diffusion process and leads to a smoother film formation. As depicted in Figure 7 the negative slope indicates a typical thermal CVD process in this regime, but occurring at lower temperatures than typical thermal CVD processes.

Based on above arguments, it can be surmised that at low temperatures, the film growth is surface reaction controlled, whereas at high temperature the growth mechanism is controlled by bulk and surface diffusion with enhanced chemical reactivity. Thus it can stated that AP-PECVD processes are similar to plasma polymerization at low temperatures, where the monomer molecules are activated by plasma and the activated molecules react/adsorb with or on the substrate depending on the surface chemistry or the surface energy, while at higher substrate temperatures the process is similar to remote plasma activated CVD, at atmospheric pressure.

To understand the excited nitrogen species present in the afterglow region of the plasma, OES analyses were carried out. OES measurements were performed in He and He + N_2 plasmas with the emission spectra depicted in Figure 8. OES spectrum of a He plasma (Figure 8a) showed the characteristic emission peaks of He at 587 nm ($2^3P \rightarrow 3^3D$), 667 nm ($2^1P \rightarrow 3^1D$), and 706.5 nm.[45,46] Figure 8b depicts the emission spectrum of He plasma diluted with 0.5 lpm of N_2. The characteristic He peak observed at 706 nm in pure He plasma diminished while typical characteristic peaks that corresponded to N, N^+, N_2, and N_2^+ were observed in the spectrum due the addition of nitrogen. It was also observed that the emission spectrum was dominated by the N_2^+ bands whose peak positions are at 337.1, 353.6, 357.7, 371.0, 375.5, 380.5, and 394.3 nm. Weak N_2^+ transitions due to Penning ionization of N_2 with He gas molecules were observed at 391.4 and 427.7 nm (see Figure 8a) were also observed.[47,48] Transitions associated with atomic nitrogen were detected, which are known to be weak compared to the radiative transitions of molecular nitrogen.[48] In the plasma, electron bombardment with molecular nitrogen can cause formation of N_2^+ and N, while the excited He interaction with N_2 (present in the ambient) *via* Penning ionization to form N_2^+ ions is clearly present in Figure 8a. The above mentioned plasma reactions can be represented by the following equations;[49]

$$N_2 + e^- \rightarrow N_2^+ + 2e^- (\text{ionization}) \quad (1)$$

$$N_2 + e^- \rightarrow 2\dot{N} + e^- (\text{dissociation}) \quad (2)$$

$$He^* + N_2 \rightarrow He + N_2^+ + e^- (\text{penning ionization}) \quad (3)$$

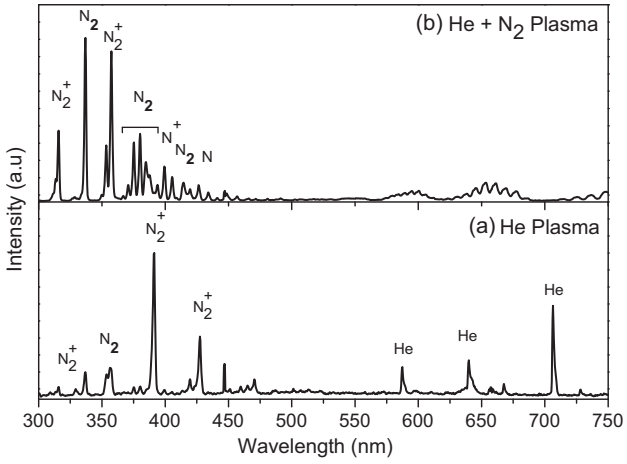

Figure 8. OES spectra (a) He and (b) He + N_2 plasma at 120 W of plasma power.

DOI: 10.1002/ppap.201100035

From the observed OES results and film properties, a possible chemical route active in the AP-PECVD process using nitrogen and TES can be suggested. The OES spectra collected in the afterglow region (where the precursor vapor is injected) of the plasma depicts the presence of activated N_2^+, N^+, and N species. These nitrogen species can react with the precursor molecule in accordance with Equation (3–5) leading to formation of $Et_3\dot{S}i_1$ radicals:

$$N_2^+ + HSiEt_3 \rightarrow Et_3\dot{S}i_1 + N_2 + H^+ \quad (4)$$

$$N^+ + HSiEt_3 \rightarrow Et_3\dot{S}i_1 + N + H^+ \quad (5)$$

$$N + HSiEt_3 \rightarrow Et_3\dot{S}i_1 + NH \quad (6)$$

As proposed by Wrobel et al.,[36] the silyl group formed in above equations may react with $HSiEt_3$ in the gas phase or with the growing film, forming a radical on the carbon atoms, as depicted in below:

$$Et_3\dot{S}i_1 + CH_3CH_2Si(Et)_2H \rightarrow (Et)_3Si{-}CH_2{-}\dot{C}H_2 \text{ (or) } (Et)_3Si{-}\dot{C}H{-}CH_3 + HSiEt_3 \quad (7)$$

The radical formed in the above reaction may undergo thermally induced decomposition at high T_s by the elimination of ethylene groups as by-product, as described below:[36]

$$\equiv Si{-}CH_2{-}\dot{C}H_2 \underset{\rightarrow}{\Delta} \equiv Si{-}H + C_2H_4 \quad (8)$$

$$\equiv Si{-}CH_2{-}CH_3 \underset{\rightarrow}{\Delta} \equiv Si{-}H + C_2H_4 \quad (9)$$

The above mentioned reactions help in the removal of organic moieties in the growing film and in our case, this occurs most effectively at $T_s \geq 250\,^{\circ}C$ leading to the formation of $Si{-}H_n$ as observed from the growth of the corresponding IR band (Figure 3).

The radical structure formed in Equation (7) may react with $Et_3\dot{S}i_1$ radical formed in Equation (4), (5), or (6), or may recombine at the growth surface as indicated below:

$$Et_3\dot{S}i_1 + \dot{C}H_2{-}CH_2{-}SiEt_2 \rightarrow Et_3Si{-}CH_2{-}CH_2{-}SiEt_3 \quad (10)$$

Similarly, two $Et_3\dot{S}i_1$ radical may combine with each other to form a disilane based moiety as shown below:

$$2(Et_3\dot{S}i_1) \rightarrow Et_3Si{-}SiEt_3 \quad (11)$$

At elevated temperatures the above formed group may react with hydrosilyl ($Si{-}H_n$) groups at the growth surface via thermally induced cross linking reaction to form [−Si−C−] network as proposed by Wrobel et al.[36]

The N_2^+, N^+, N species produced in the plasma and the reactive H (formed as the byproducts from $HSiEt_3$,) can form reactive amino group (NH) (by-product of Equation 6) and other reactive products as depicted below:

$$N_2^+ + H \rightarrow N_2H^+ \quad (12)$$

$$N^+ + H \rightarrow NH^+ \quad (13)$$

The NH group and the reactive N can react with $(Et)_3Si{-}CH_2{-}\dot{C}H_2$ (Equation 7) at the growing surface as shown below:[6]

$$NH + (Et)_3Si{-}CH_2{-}\dot{C}H_2 \rightarrow (Et)_3Si{-}NH{-}CH_2{-}\dot{C}H_2 \quad (14)$$

$$N + Et_3\dot{S}i_1 \rightarrow Et_2\dot{S}i_1{-}CN + C_2H_4 + H_2 \quad (15)$$

The organic moieties that are attached to the product that is formed in the above equation may undergo thermally induced desorption at higher T_s leading to the formation of Si−N and Si−C−N networks via crosslinking.

Similarly the hydrosilyl group formed as the product of the radicals shown in Equation (10) and (11) may readily react with NH as depicted below:

$$Si{-}H_n + NH \rightarrow \equiv Si{-}NH + H_n \quad (16)$$

This group may undergo crosslinking reaction with other carbosilane groups leading to the formation of complex a-SiCN:H films. The observed decrease in $Si{-}H_n$ intensity and increase in the absorption of SiC/Si−N at $T_s \geq 350\,^{\circ}C$ suggest the possibility of the above mentioned reactions.[6]

Also NH group incorporation in the $Et_3\dot{S}i_1$ groups can occur at the growth surface as depicted below:

$$NH + Et_3\dot{S}i_1 \rightarrow [Et_3SiNH]^{\bullet} \quad (17)$$

$$[Et_3SiNH]^{\bullet} + Et_3\dot{S}i_1 \rightarrow Et_3Si{-}N(H){-}SiEt_3 \quad (18)$$

$$Et_3Si{-}N(H){-}SiEt_3 \rightarrow (Et)_3Si{-}N(H){-}Si(Et_3)_2{-}CH_2{-}\dot{C}H_2 \quad (19)$$

The products formed in the above equations may undergo thermally activated decomposition at higher T_s to form Si−N and Si−C−N based network via elimination of organic moieties and cross-linking reaction as discussed earlier which correlate well with observations made from XPS and FTIR spectroscopic techniques.

From the discussions and the experimental observations at low T_s, the activated $HSiEt_3$ molecules and the NH species

(formed as a byproduct of the gas-phase reactions) become adsorbed on the substrate with minimum reactivity. As the T_s increases to 250 °C the 1,1-diethyl-2-methysilene molecule desorbs the ethyl and ethylene groups leading to the formation of Si—H_n as evident from the FTIR analysis. Reaction between the Si—H_n and the NH becomes more probable at T_s above 350 °C leading to the formation of complex a-SiCN:H ceramic like films.

4. Conclusion

a-SiCN:H films were deposited on c-Si using AP-PECVD with TES and nitrogen. The substrate temperature plays a crucial role in controlling the structure and the chemical composition of a-SiCN:H films. The increase in T_s eliminates the organic moieties and incorporates more nitrogen in the film leading to the formation of ceramic like film structure. Film growth rate showed strong dependence on the T_s. Between 25 and 250 °C the film thickness decreased with an increase in T_s, which showed the film growth mechanism was surface reaction controlled, while between 250 and 425 °C the film thickness increased which indicated that film growth mechanism is mass-transport controlled. No film formation was observed without N_2 addition to the plasma gas (He), which indicated AP-PECVD was a radical initiated process. From the depicted possible chemical reactions it can be concluded that the nitrogen reactive species in the after-glow region of the plasma initiated the fragmentation of the $HSiEt_3$, which on subsequent reaction in the gas-phase and on the substrate with NH species leads to the formation of a-SiCN:H films whose structure and properties strongly depend on the T_s.

Acknowledgements: This material is based on research sponsored by the Department of Energy grant DE-FG36-08GO88160. The views and conclusions contained herein are those of the authors and should not be interpreted as necessarily representing the official policies or endorsements, either expressed or implied of the Department of Energy or the U.S. Government. Authors would like to thank Drs. D. L. Schulz, S. Elangovan, and G. R. S. Iyer for their constructive suggestions and comments. Help from Ms. H. Doktor and Mr. J. Risan (MCAL) and Mr. S. Payne (Electron Microscopy Center, NDSU) for their assistance in FTIR, NI, and SEM characterizations, respectively, are greatly appreciated. XPS measurements were carried out in the Characterization Facility, University of Minnesota, as part of the NSF-funded Materials Research Facilities Network and funded by the National Science Foundation (NSF) through the University of Minnesota Materials Research Science and Engineering Center (MRSEC) Materials Research Facilities Network (MRFN) supplemental funding award. The authors would like to gratefully acknowledge Dr. Bing Luo, Dr. Timothy Lodge, Dr. John Nelson, Alice Ressler, and Sharon Emde for this opportunity.

Received: February 17, 2011; Revised: June 27, 2011; Accepted: July 18, 2011; DOI: 10.1002/ppap.201100035

Keywords: atmospheric pressure glow discharge; atmospheric pressure plasma enhanced chemical vapor deposition (AP-PECVD); plasma-precursor interaction and growth kinetics; remote plasma

[1] S. Guruvenket, M. Azzi, D. Li, J. A. Szpunar, L. Martinu, J. E. Klemberg-Sapieha, *Surf. Coat. Technol.* **2010**, *204*, 3358.
[2] B. Sopori, *J. Electron. Mater.* **2005**, *34*, 564.
[3] C. C. Chiang, M. C. Chen, C. C. Ko, S. M. Jang, C. H. Yu, M. S. Liang, *Jpn. J Appl. Phys 1* **2003**, *42*, 5246.
[4] D. Li, S. Guruvenket, M. Azzi, J. A. Szpunar, J. E. Klemberg-Sapieha, L. Martinu, *Surf. Coat. Technol.* **2010**, *204*, 1616.
[5] N. Cherault, G. Carlotti, N. Casanova, P. Gergaud, C. Goldberg, O. Thomas, M. Verdier, *Microelectron. Eng.* **2005**, *82*, 368.
[6] A. M. Wrobel, I. Blaszczyk-Lezak, A. Walkiewicz-Pietrzykowska, *J. Appl. Polym. Sci.* **2007**, *105*, 122.
[7] A. M. Wrobel, I. Blaszczyk-Lezak, A. Walkiewicz-Pietrzykowska, T. Aoki, J. Kulpinskic, *J. Electrochem. Soc.* **2008**, *155*, K66.
[8] A. M. Wrobel, I. Blaszczyk-Lezak, A. Walkiewicz-Pietrzykowska, D. M. Bielinski, T. Aoki, Y. Hatanaka, *J. Electrochem. Soc.* **2004**, *151*, C723.
[9] A. M. Wrobel, A. Walkiewicz-Pietrzykowska, I. Blaszczyk-Lezak, *Appl. Organomet. Chem.* **2010**, *24*, 201.
[10] I. Blaszczyk-Lezak, A. M. Wrobel, D. M. Bielinski, *Diamond Relat. Mater.* **2006**, *15*, 1650.
[11] E. Gonzalez, M. D. Barankin, P. C. Guschl, R. F. Hicks, *Langmuir* **2008**, *24*, 12636.
[12] F. Fanelli, R. d'Agostino, F. Fracassi, *Plasma Process. Polym.* **2007**, *4*, 797.
[13] F. Fanelli, F. Fracassi, R. d'Agostino, *Surf. Coat. Technol.* **2010**, *204*, 1779.
[14] L. Bárdos, H. Baránková, *Thin Solid Films* **2010**, *518*, 6705.
[15] V. Raballand, J. Benedikt, S. Hoffmann, M. Zimmermann, A. von Keudell, *J. Appl. Phys.* **2009**, *105*, 083304.
[16] V. Raballand, J. Benedikt, A. von Keudell, *Appl. Phys. Lett.* **2008**, *92*, 091502.
[17] V. Hopfe, D. W. Sheel, *Plasma Process. Polym.* **2007**, *4*, 253.
[18] V. Hopfe, D. W. Sheel, *IEE Trans. Plasma Sci.* **2007**, *35*, 204.
[19] V. Hopfe, R. Spitzl, I. Dani, G. Maeder, L. Roch, D. Rogler, B. Leupolt, B. Schoeneich, *Chem. Vapor. Depos.* **2005**, *11*, 497.
[20] G. R. Nowling, S. E. Babayan, V. Jankovic, R. F. Hicks, *Plasma Sources Sci.* **2002**, *11*, 97.
[21] G. R. Nowling, S. E. Babayan, X. Yang, M. Moravej, R. Agarwal, R. F. Hicks, *Plasma Sources Sci.* **2004**, *13*, 156.
[22] A. M. Ladwig, R. D. Koch, E. G. Wenski, R. F. Hicks, *Diamond Relat. Mater.* **2009**, *18*, 1129.
[23] K. W. Johnson, S. Jha, C. Braun, K. Anderson, B. Halverson, K. Pokhodnya, S. Guruvenket, R. A. Sailer, D. L. Schulz, 52nd Annual Technical Conference Proceedings, Society of Vacuum Coaters, 2009, 327.
[24] K. W. Johnson, S. Guruvenket, S. Jha, B. Halverson, C. Olson, R. A. Sailer, D. L. Schulz, 34th IEEE Photovoltaic Specialists Conference, 2009, 001806.
[25] R. A. Sailer, A. Wagner, C. Schmit, N. Klaverkamp, D. L. Schulz, *Surf. Coat. Technol.* **2008**, *203*, 835.
[26] M. D. Barankin, E. Gonzalez, A. M. Ladwig, R. F. Hicks, *Sol. Energy Mater. Sol. Cells* **2007**, *91*, 924.
[27] M. Moravej, R. F. Hicks, *Chem. Vapor. Depos.* **2005**, *11*, 469.
[28] W. C. Oliver, G. M. Pharr, *J. Mater. Res.* **1992**, *7*, 1564.
[29] S. Guruvenket, J. Ghatak, P. V. Satyam, G. M. Rao, *Thin Solid Films* **2005**, *478*, 256.

DOI: 10.1002/ppap.201100035

[30] A. Amassian, R. Vernhes, J. E. Klemberg-Sapieha, P. Desjardins, L. Martinu, *Thin Solid Films* **2004**, *469-70*, 47.
[31] Z. L. Fang, *Surf. Coat. Technol.* **2008**, *202*, 4198.
[32] M. Ohring, *Materials Science of Thin Films — Deposition and Structure*, 2nd edition, Academic Press, New York, USA, **2002**.
[33] Y. Awad, M. A. El Khakani, C. Aktik, J. Mouine, N. Camire, M. Lessard, M. Scarlete, H. A. Al-Abadleh, R. Smirani, *Surf. Coat. Technol.* **2009**, *204*, 539.
[34] D. S. Kim, Y. H. Lee, *Thin Solid Films* **1996**, *283*, 109.
[35] R. Di Mundo, M. Ricci, R. d'Agostino, F. Fracassi, F. Palumbo, *Plasma Process. Polym.* **2007**, *4*, S21.
[36] A. M. Wrobel, A. Walkiewicz-Pietrzykowska, M. Ahola, I. J. Vayrynen, F. J. Ferrer-Fernandez, A. R. Gonzalez-Elipe, *Chem. Vapor. Depos.* **2009**, *15*, 39.
[37] E. Gat, M. A. Elkhakani, M. Chaker, A. Jean, S. Boily, H. Pepin, J. C. Kieffer, J. Durand, B. Cros, F. Rousseaux, S. Gujrathi, *J. Mater. Res.* **1992**, *7*, 2478.
[38] F. J. Gomez, P. Prieto, E. Elizalde, J. Piqueras, *Appl. Phys. Lett.* **1996**, *69*, 773.
[39] P. Jedrzejowski, J. Cizek, A. Amassian, J. E. Klemberg-Sapieha, J. Vlcek, L. Martinu, *Thin Solid Films* **2004**, *447*, 201.
[40] Y. Awad, M. A. El Khakani, M. Scarlete, C. Aktik, R. Smirani, N. Camire, M. Lessard, J. Mouine, *J. Appl. Phys.* **2010**, *107*, 033517.
[41] X. M. He, T. N. Taylor, R. S. Lillard, K. C. Walter, M. Nastasi, *J. Phys.:Condens. Matter* **2000**, *12*, 8937.
[42] Y. Awad, M. A. El Khakani, D. Brassard, R. Smirani, N. Camire, M. Lessard, C. Aktik, M. Scarlete, J. Mouine, *Thin Solid Films* **2010**, *518*, 2738.
[43] J. Niemann, W. Bauhofer, *Thin Solid Films* **1999**, *352*, 249.
[44] J. W. Sun, Y. F. Zhang, D. Y. He, *Diamond Relat. Mater.* **2000**, *9*, 1668.
[45] J. L. Walsh, J. J. Shi, M. G. Kong, *Appl. Phys. Lett.* **2006**, *89*, 171501.
[46] V. Leveille, S. Coulombe, *Plasma Sources Sci.* **2005**, *14*, 467.
[47] W. C. Zhu, Q. Li, X. M. Zhu, Y. K. Pu, *J. Phys. D Appl. Phys.* **2009**, *42*, 202002.
[48] A. J. Wagner, D. H. Fairbrother, F. Reniers, *Plasma Polym.* **2003**, *8*, 119.
[49] A. M. Wrobel, I. Blaszczyk, A. Walkiewicz-Pietrzykowska, A. Tracz, J. E. Klembrg-Sapieha, T. Aoki, Y. Hatanaka, *J. Mater. Chem.* **2003**, *13*, 731.